







Cite this: *Nanoscale*, 2018, **10**, 1540

## Metallic impurities in black phosphorus nanoflakes prepared by different synthetic routes†

Carmen C. Mayorga-Martinez, <sup>a</sup> Zdeněk Sofer, <sup>b</sup> David Sedmidubský, <sup>b</sup>  
Jan Luxa,<sup>b</sup> Bahareh Kherzi<sup>a</sup> and Martin Pumera <sup>\*a,b</sup>

The allotropes of elementary phosphorus materials, such as black phosphorus and its single layer form phosphorene have recently regained scientific attention due to their outstanding properties suitable for applications in electronics, optical devices, and energy applications. As with many other materials, there is a fundamental question of the presence of impurities in these materials and their influence on the properties. Such impurities are expected to dramatically influence the electronic and electrochemical properties of black phosphorus in a way similar to the way they do in the case of graphene. Here, we synthesize black phosphorus from commercially available red phosphorus *via* different techniques. We utilize high-pressure conversion of red phosphorus to black phosphorus and vapor phase growth of black phosphorus using a gold/tin alloy-like solvent for red phosphorus. We show that both methods lead to black phosphorus containing a large number of metallic impurities. We show that the classical tin-based method for preparing black phosphorus adds a significant amount of tin and that the metallic impurities present have an observable effect on the electrochemical properties of black phosphorus.

Received 3rd August 2017,  
Accepted 8th December 2017

DOI: 10.1039/c7nr05718k

rscl.li/nanoscale

### Introduction

Black phosphorus has attracted scientific attention as this material is an elemental solid and individual layers are held together by weak van der Waals interactions to create a crystal with orthorhombic symmetry.<sup>1–3</sup> Black phosphorus can therefore be exfoliated to few or single layered phosphorene, in a similar manner of graphite to graphene or bulk MoS<sub>2</sub> to its single layer form. Black phosphorus was first prepared more than 100 years ago using a high hydrostatic pressure of 1.2 GPa at 200 °C within 5–30 min.<sup>4</sup> More than sixty years ago the first “low pressure” synthesis procedure was developed based on the catalytic conversion of white phosphorus with mercury<sup>5</sup> and recently also a new method using Sn–Au alloys as well as pure Sn in the presence of SnI<sub>4</sub> based on the vapour transport growth method was developed.<sup>6–8</sup> Black phosphorus remained a scientific curiosity for almost a hundred years, until recently when it was reported to have potential applications in photocatalysis<sup>9–11</sup> semiconductors,<sup>12</sup> rechargeable batteries<sup>13</sup> and (bio)sensing.<sup>14–16</sup> There are several methods

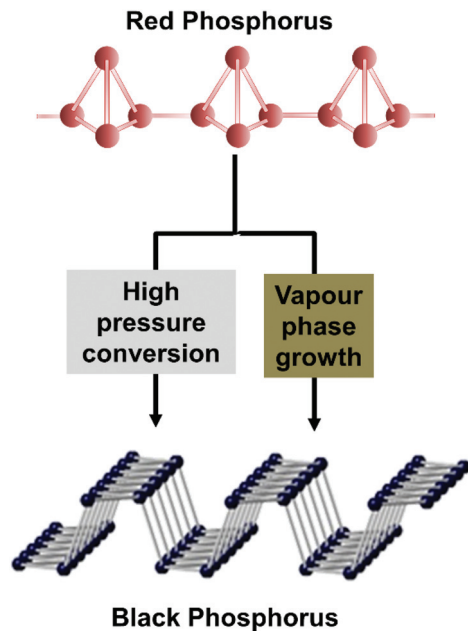
that are used for the preparation of black phosphorus, such as high pressure or Au/Sn alloy based vapour phase growth using red phosphorus as a precursor. White, black and red phosphorus are allotropes of elemental phosphorus. Each allotrope exhibits different crystal structures: white phosphorus displays a cubic structure, while red phosphorus is amorphous and black phosphorus has an orthorhombic structure. Single layer black phosphorus has recently been termed phosphorene to show its relationship with 2D graphene (although in the case of BP the suffix “-ene” has no nomenclature support). Despite the fact that BP does not show aromaticity or single atom thickness as graphene, it has something else in common with graphene as we report below. It was believed for many years that graphene is a pure material and it was found only later that the graphene contains metallic impurities, either originating from graphite as a source material,<sup>17,18</sup> from the catalyst in the case of CVD graphene<sup>19,20</sup> or from the chemicals (and impurities in these chemicals) used for graphene preparation.<sup>21,22</sup> It was shown that these metallic impurities dramatically influence its catalytic<sup>21,23</sup> and electronic properties.<sup>20</sup> Graphene, in many ways, followed the previous example of carbon nanotubes.<sup>12,22</sup> In a similar way, it was demonstrated that MoS<sub>2</sub> contains many impurities<sup>24–29</sup> which originate from the natural mineral of MoS<sub>2</sub> or from the synthetic precursors of MoS<sub>2</sub>. These impurities influence the electronic and catalytic properties of MoS<sub>2</sub>.<sup>30,31</sup> Having these examples of layered and 2D materials in mind and given the explosive growth of black phosphorus applications in many areas, from electronic, to optical to

<sup>a</sup>Division of Chemistry & Biological Chemistry, School of Physical Mathematical Science, Nanyang Technological University, Singapore 637371, Singapore.  
E-mail: pumera.research@gmail.com

<sup>b</sup>Department of Inorganic Chemistry, University of Chemistry and Technology Prague Technická 5, 166 28 Prague 6, Czech Republic

†Electronic supplementary information (ESI) available. See DOI: 10.1039/c7nr05718k





**Scheme 1** Crystal structure and synthesis methods used for the production of black phosphorus from red phosphorus.

electrochemical applications, one would be curious to know whether there are any impurities in black phosphorus and whether they have any influence on its properties.

Here we prepare black phosphorus (BP) by two fundamentally different routes, high pressure conversion (HPC) or vapour phase growth (VPG) using Au/Sn as a solvent (Scheme 1). In both cases, highly pure red phosphorus is used as a precursor. We show that indeed, there is a significant amount of metallic impurities in black phosphorus, and we demonstrate that the impurities influence its electrochemical properties. These findings are of immense conceptual importance when discussing the fabrication of black phosphorus derived devices.

## Experimental section

### Materials

Red phosphorus (99.999%) and tin (99.999%) were obtained from Sigma-Aldrich (Czech Republic). Iodine (99.9%), carbon disulfide (99.99%) and chloroform (99.9%) were obtained from Penta, Czech Republic. Gold (99.99%) was obtained from Safina, Czech Republic.

**Synthesis of black phosphorus materials.** Black phosphorus materials were synthesized using two methods, high pressure conversion<sup>3</sup> (BP HPC) and vapour phase growth<sup>8</sup> (BP VPG), in both cases high purity chemical reagents were used.

For the first method, 10 g of red phosphorus was wrapped in graphite foil and was exposed to high pressure (6 GPa) and temperature (600 °C) conditions using uniaxial pressing apparatus of 1" size, followed by slowly cooling (100 °C min<sup>-1</sup>) to

room temperature. Finally, the resulting ceramic piece (20 mm × 5 mm) was mechanically removed from the graphite foil. For the preparation of BP using the second method, we followed the method reported by Lange *et al.* in 2007<sup>6</sup> and modified by our group.<sup>8</sup> 500 mg of Au/Sn alloy (prepared by melting stoichiometric amounts of tin and gold under high vacuum), 15 mg SnI<sub>4</sub> and 720 mg of red phosphorus were placed inside a quartz ampoule, followed by sealing of the ampoule using an oxygen/hydrogen torch. Subsequently, the ampoule was heated at 400 °C for 1 hour using a muffle furnace and kept in these conditions for two more hours. After that the temperature was increased until 600 °C for 24 h. Finally, the muffle furnace was cooled to room temperature overnight, and then the resulting plates (up to 5 mm × 2 mm) were washed with CS<sub>2</sub> to remove the remaining white phosphorus<sup>32</sup> and SnI<sub>4</sub><sup>33</sup> formed during the synthesis. For the preparation of SnI<sub>4</sub>, iodine and tin in chloroform was placed under reflux followed by the purification of SnI<sub>4</sub> obtained by recrystallization from chloroform. After the materials were synthesized, a solution of 5 mg mL<sup>-1</sup> of each material was prepared and subjected to sonication for 6 hours to obtain a good nanosheet dispersion.

**Characterization.** The characterisation of the chemical composition of phosphorus allotropes was performed using an X-ray photoelectron spectrometer (Phoibos 100 spectrometer and a monochromatic Mg X-ray radiation source, SPECS, Germany) and a confocal micro-Raman spectrometer (LabRam HR instrument, Horiba Scientific). X-ray diffraction (XRD) was performed with a Bruker D8 Discoverer diffractometer in the Bragg–Brentano para-focusing geometry. Cu K $\alpha$  radiation was used. Diffraction patterns were collected between 10° and 80° of 2 $\theta$ . The obtained data were evaluated using HighScore Plus 3.0e software. High resolution transmission electron microscopy (HR-TEM) was performed using an EFTEM Jeol 2200 FS microscope (Jeol, Japan). A 200 keV acceleration voltage was used for measurement. Sample preparation was attained by drop casting the suspension (1 mg mL<sup>-1</sup>) on a TEM grid (Cu; 200 mesh; formvar/carbon) and drying at 60 °C for 12 h. Trace metal analysis was performed by inductively coupled plasma mass spectrometry (ICP-MS), using an Agilent 7700x system (Japan). Prior to analysis, samples were digested with HNO<sub>3</sub> using a Milestone Ethos one microwave digestion system (Italy).

**Electrochemical measurements.** For the electrochemical measurements, a compact and modular potentiostat/galvanostat (Autolab PGSTAT204/FRA32 M. Eco Chemie, Utrecht, The Netherlands) controlled by NOVA Version 1.1 software (Eco Chemie) and a three electrode (glassy carbon (GC) electrode as the working electrode-WE, counter electrode-CE and Ag/AgCl reference electrode-RE) system were used. Prior to each electrochemical study, a GC electrode of 3 mm in diameter (WE) was modified with 15  $\mu$ g of the desired material by drop casting. Linear sweep voltammetry (LSV) was performed in 0.5 M H<sub>2</sub>SO<sub>4</sub> using a scan rate of 2 mV s<sup>-1</sup> for the hydrogen evolution reaction. Cyclic voltammograms were recorded from Ni impurities using a scan rate of 100 mV s<sup>-1</sup>. LSV measurements were performed vs. Ag/AgCl and the obtained potentials were con-



verted to the reversible hydrogen electrode (RHE) scale according to the Nernst equation:

$$E_{\text{RHE}} = E_{\text{Ag/AgCl}} + 0.059\text{pH} + E_{\text{Ag/AgCl}}^{\circ}$$

where  $E_{\text{Ag/AgCl}}^{\circ} = 0.1976$  at 25 °C

## Results and discussion

After black phosphorus materials were synthesized using high purity chemical reagents by high pressure conversion and vapor phase growth synthesis (Scheme 1), we characterized the resulting black phosphorus materials with a variety of methods, including scanning electron microscopy (SEM), transmission electron microscopy (TEM), X-ray diffraction (XRD), X-ray photoelectron spectroscopy (XPS) and inductively coupled plasma mass spectrometry (ICP-MS).

The morphology of black phosphorus prepared by high pressure conversion (BP HPC) and vapor phase growth (BP VPG) synthesis was studied by SEM (Fig. 1). The layered morphology is clearly visible only for black phosphorus prepared by vapour phase growth. The layered morphology was not

clearly observed for black phosphorus prepared by high pressure synthesis, which is also indicated by the broadening of the X-ray diffraction patterns due to its nanocrystalline structure as discussed below. For comparison, the SEM image of amorphous red phosphorus used as a starting material is also shown in Fig. 1.

Once we confirmed that the BP materials were successfully synthesized, the materials were mechanically exfoliated by mild ultrasonic treatment for 6 hours. We used TEM to further investigate the crystallinity of the exfoliated BP nanoflakes. High-resolution TEM (HR-TEM) images and selective area electron diffraction (SAED) patterns show the orthorhombic crystalline nature of the investigated black phosphorus materials (see Fig. 2).

The phase composition of BP HPC and BP VPG was proved by X-ray diffraction. Both the black phosphorus samples prepared by vapour growth and high pressure synthesis show an orthorhombic structure (*Cmca* space group; PDF card # 01-076-1957). Vapour phase growth phosphorus (BP VPG) shows strong preferential orientation along the  $(0k0)$  direction and an extremely narrow diffraction pattern. This indicates the high crystallinity of the material obtained by vapour phase growth and is in good agreement with the observed layered structure by SEM. It was observed that the black phosphorus samples prepared by high pressure synthesis show the significant broadening of all diffraction patterns and only minimal preferential orientation originating from the layered structure. This shows the nanocrystalline character of black phosphorus prepared by high pressure synthesis, in the range of tenths of nanometers corresponding to tenths to hundreds of BP layers. For comparison the diffractogram of amorphous red phosphorus used as a starting material is also shown. The red phosphorus is clearly amorphous. The observed broad diffraction patterns are typical of an amorphous material and corres-

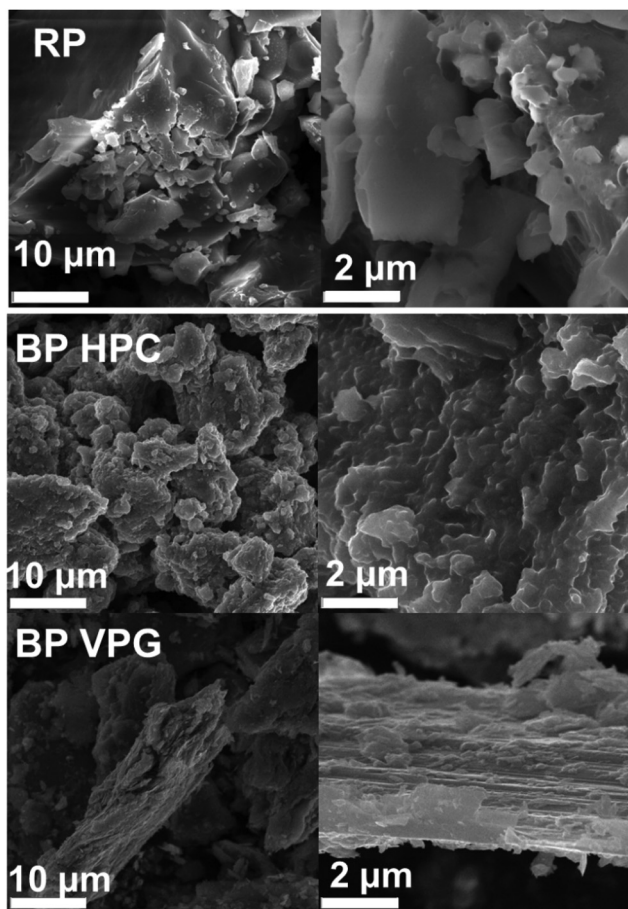


Fig. 1 The SEM images at different magnifications of red phosphorus (RP), black phosphorus prepared by high-pressure conversion (BP HPC) and vapour phase growth (BP VPG) synthesis.

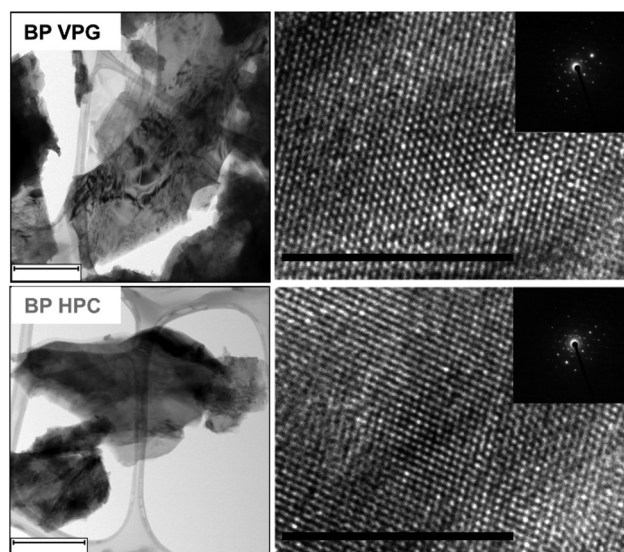


Fig. 2 The TEM images (left) and HR-TEM images (right) with the corresponding SAED (insert) of BP HPC and BP VPG nanoflakes. The scale bar corresponds to 500 nm (TEM images) and 10 nm (HR-TEM).



pond to the average inter-atomic distances on short range ordering (chemical bonds in the glass state material; *e.g.* P<sub>4</sub> tetrahedra forming amorphous red phosphorus). The X-ray diffractograms are shown in Fig. 3A.

Furthermore, the prepared BP materials mechanically exfoliated by mild ultrasonic treatment for 6 hours were characterized by X-ray photoelectron spectroscopy (XPS) in order to obtain the detailed information on the chemical composition of their structure and the chemical bonds present. The BP VPG, BP HPC, as well as the precursor RP as the reference were investigated. Fig. 3B shows the high resolution XPS spectrum of the P 2p core level for all the elemental phosphorus allotropes. The characteristic binding energies of two features in the regions of P 2p that correspond to P–P bonding were observed for both black phosphorus materials (VPG and VPC). While for the commercial red phosphorus only one feature was obtained, and the data are in good agreement with the literature.<sup>1</sup> The surface oxidation features were observed in all

the materials at 134 ± 0.6 eV, being more evident in RP. The oxidative feature observed on the materials is due to low stability and easy passivation of the phosphorus allotropes in water solution.<sup>34</sup> Moreover, energy-dispersive X-ray (EDX) spectra were recorded for both BP materials (VPG and HPC) immediately after the synthesis and before being subjected to mechanical exfoliation. The EDX analysis for the commercial RP before dissolving in water by sonication was performed as well (see Fig. S1 in the ESI†). These measurements confirm the absence of oxygen in the commercial red phosphorus; oxygen was introduced during the dissolution by sonication.

Later Raman spectroscopy was performed for the BP materials evaluated in this study, see Fig. 3C. The Raman spectra of BP VPG show the characteristic intensities of A<sub>1g</sub>, B<sub>2g</sub>, and A<sub>2g</sub> at 360 cm<sup>-1</sup>, 440 cm<sup>-1</sup> and 465 cm<sup>-1</sup> respectively, while for the BP HPC the intensities were at 362.5 cm<sup>-1</sup> (A<sub>1g</sub>), 440 cm<sup>-1</sup> (B<sub>2g</sub>) and 465 cm<sup>-1</sup> (A<sub>2g</sub>).<sup>35–38</sup> The Raman spectrum of RP shows a typical peak of amorphous red phosphorus.<sup>39</sup>

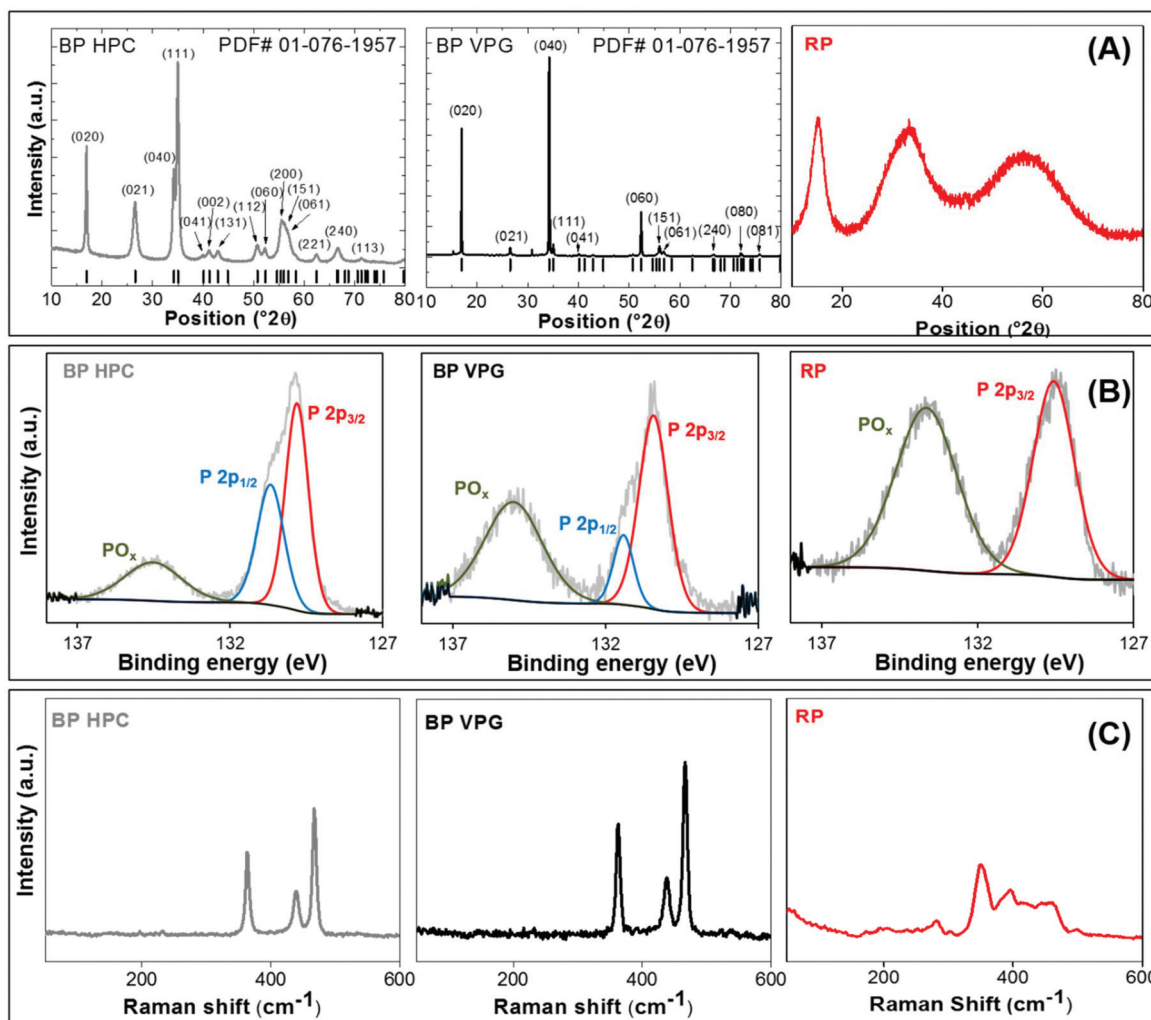


Fig. 3 X-ray diffractogram (A), high resolution XPS spectrum of the P 2p core level (B) and Raman spectra (C) of black phosphorus prepared by vapour phase growth (BP VPG), black phosphorus produced by high pressure conversion (BP HPC), and commercial amorphous red phosphorus (RP) used as a precursor for the synthesis.



The metal impurities were quantified using inductively coupled plasma mass spectrometry (ICP-MS). Interestingly, the ICP-MS results of the starting material commercial red phosphorus (with a nominal purity of 99.999%) show the content of some metal impurities such as Cr (41 ppm), Fe (51 ppm), Ni (317 ppm), Cu (147 ppm), Zn (121 ppm), Sn (77 ppm) and Pb (44 ppm). As we can see in Table 1, the amount of Fe, Cu and Zn impurities increased significantly after RP was exposed to high pressure and vapour phase growth methods to obtain BP.

However, the Ni content increased for the BP VPG and decreased for BP HPC. Although we used reagents of high purity, the resulting materials have a high content of metallic impurities such as Fe, Ni, Cu, Zn and Sn; also the presence of iodine was observed. Particularly, in the BP vapor phase growth the Sn and I impurities came from Sn and SnI<sub>4</sub> used during the synthesis and remained even after washing with CS<sub>2</sub>. In the case of BP prepared by high pressure conversion the metal impurities came from the high pressure system used for the synthesis and packing in graphite foil used as a vessel for such synthesis.

Subsequently, we were interested in investigating if the metallic impurities had an influence on the electrochemical properties of the materials. It is known that some of the transition metals show the inherent electrochemical signature

originating from their oxidation/reduction.<sup>39</sup> These include Ni, which is present as an impurity in BP, see Table 1. We investigated whether Ni impurities influence the voltammetric signature of black phosphorus. Fig. 4 shows the CV recorded in alkali media of GC electrodes modified with 5 μg of BP VGP, BP HPC and RP materials; NiO NPs were also tested for com-

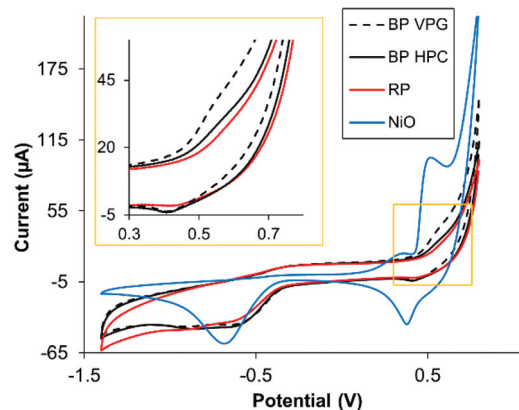


Fig. 4 Overlay of the 20th CV scan of NiO NPs and BP VPG, BP HPC and RP in 0.1 M NaOH, scan rate: 0.1 V s<sup>-1</sup>, GC electrodes (3 mm of diameter) were modified with the materials under study.

Table 1 Impurity content in BP VPG, BP HPC, VP and RP quantified by ICP-MS. Values are in ppm units

																	He
												B	C	N	O	F	Ne
												0					
												0					
												0					
												Al	Si	P	S	Cl	Ar
												40					
												270					
												0					
H																He	
Li	Be																
Na	Mg																
	122																
	315																
	28																
K	Ca	Sc	Ti	V	Cr	Mn	Fe	Co	Ni	Cu	Zn	Ga	Ge	As	Se	Br	Kr
	0				30	0	361	0	422	1021	451						
	0				75	0	1802	0	135	1185	435						
	148				41	0	51	0	317	147	121						
Rb	Sr	Y	Zr	Nb	Mo	Tc	Ru	Rh	Pd	Ag	Cd	In	Sn	Sb	Te	I	Xe
											0		2520			2568	
											0		0			0	
											0		77			0	
Cs	Ba	La	Hf	Ta	W	Re	Os	Ir	Pt	Au	Hg	Tl	Pb	Bi	Po	At	Rn
	0												0				
	0												0				
	0												44				

Ce	Pr	Nd	Pm	Sm	Eu	Gd	Tb	Dy	Ho	Er	Tm	Yb	Lu
Th	Pa	U	Np	Pu	Am	Cm	Bk	Cf	Es	Fm	Md	No	Lr



parison. After 20 continuous voltammetric scans, the oxidative and reductive peaks were observed in the BP VPG and BP HPC materials. Fig. 4 shows the 20th scan, where the oxidation peak intensity constantly reaching an almost stable contour. The potentials of these peaks corresponding to  $\text{Ni}(\text{OH})_2/\text{NiOOH}$  were observed, as confirmed by comparison with NiO NPs (Fig. 4, blue line).<sup>22,40</sup>

In addition, some of the transition metals exhibit a catalytic effect on the hydrogen evolution reaction whilst black phosphorus is not particularly catalytic for hydrogen evolution.<sup>3</sup> Differences between different BP materials in their HER activities may serve as an indicator of impurities. We observed that the BP HPC and BP VPG show different hydrogen evolution reactions (HERs) (Fig. 5A); BP HPC shows higher HER electrocatalysis than BP VPG. Interestingly, the BP obtained using the HPC method shows a higher content of Fe impurity than the BP obtained by the VGP method (Table 1). Therefore, we also evaluated the HER performance of  $\text{Fe}_3\text{O}_4$  which catalyzes HER. We therefore show the direct relationship between the Fe based impurities in BP and its HER catalysis. Moreover, a slight improvement in the HER of RP is observed, this performance was reported before, where RP was used for visible light driven photocatalytic  $\text{H}_2$  formation from water.<sup>9</sup>

Moreover, to elucidate the electrochemical mechanisms, Tafel analysis is executed (Fig. 5B). The mechanisms of the hydrogen evolution on black phosphorus materials, red phosphorus and  $\text{Fe}_3\text{O}_4$  surfaces are in agreement with the Volmer adsorption step.

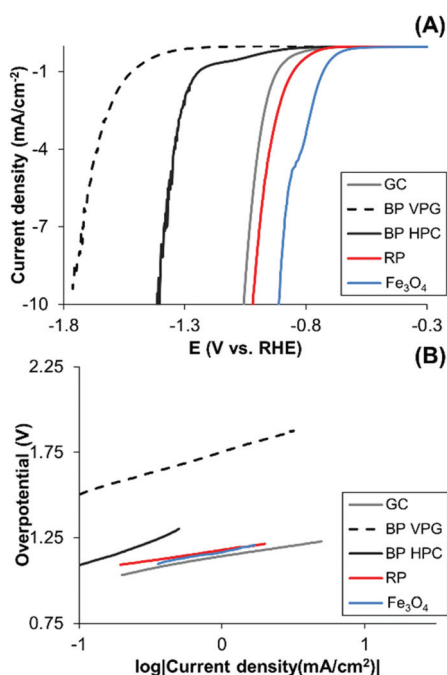


**Fig. 5** Hydrogen evolution reaction (HER) performed in 0.5 M  $\text{H}_2\text{SO}_4$  solution. Linear sweep voltammetry (A) and Tafel plot (B) of BP VPG, BP HPC, RP GC bare and  $\text{Fe}_3\text{O}_4$ . Glassy carbon electrodes (3 mm of diameter) were modified with the materials under study.

## Conclusion

In summary in this study, we have demonstrated that different synthetic routes (high pressure conversion and vapor phase growth) to black phosphorus introduce or retain different metal impurities. We found that there are impurities in the resulting black phosphorus, which originate from the impurities in the starting red phosphorus and from the agents used for the synthesis of black phosphorus, such as Sn alloy. We demonstrated that metallic impurities, in this case Ni and Fe based, influence the electrochemical response of black phosphorus. Both synthetic methods retain the impurity from the red phosphorus (precursor), Ni, that influences the voltammetric signature of black phosphorus. Fe impurities are introduced during both synthetic methods. The high pressure conversion route introduces a higher amount of Fe impurities that results in a larger catalytic influence upon HER. This study serves as a warning to researchers working in the field of black phosphorus and phosphorene as metal impurities in general influence not only the electrochemical properties but may also influence the electronic and other properties of black phosphorus-derived materials.

## Conflicts of interest

There are no conflicts to declare.

## Acknowledgements

M. P. thanks the Tier 1 fund (01/13). Z. S., D. S. and J. L. were supported by the Czech Science Foundation (GACR No. 15-09001S) and by the specific university research (MSMT No. 20-SVV/2017). This work was performed with the financial support from the Neuron Foundation for science support. This work was supported by the project Advanced Functional Nanorobots (Reg. No. CZ.02.1.01/0.0/0.0/15\_003/0000444 financed by the EFRR).

## Notes and references

- N. B. Goodman, L. Ley and D. W. Bullett, *Phys. Rev. B: Condens. Matter Mater. Phys.*, 1983, **27**, 7440–7450.
- S. H. Aldave, M. N. Yogeesh, W. Zhu, J. Kim, S. S. Sonde, A. P. Nayak and D. Akinwande, *2D Mater.*, 2016, **3**, 014007.
- Z. Sofer, D. Sedmidubsky, S. Huber, J. Luxa, D. Bousa, C. Boothroyd and M. Pumera, *Angew. Chem., Int. Ed.*, 2016, **55**, 3382–3386.
- P. W. Bridgman, *J. Am. Chem. Soc.*, 1914, **36**, 1344–1363.
- H. Krebs, H. Weitz and K. H. Worms, *Z. Anorg. Allg. Chem.*, 1955, **280**, 119–133.
- S. Lange, P. Schmidt and T. Nilges, *Inorg. Chem.*, 2007, **46**, 4028–4035.



- 7 M. Kopf, N. Eckstein, D. Pfister, C. Grotz, I. Kruger, M. Greiwe, T. Hansen, H. Kohlmann and T. J. Nilges, *Cryst. Growth*, 2014, **405**, 6–10.
- 8 C. C. Mayorga-Martinez, Z. Sofer and M. Pumera, *Angew. Chem., Int. Ed.*, 2015, **127**, 14525–14528.
- 9 F. Wang, W. K. H. Ng, J. C. Yu, H. Zhu, C. Li, L. Zhang, Z. Liu and Q. Li, *Appl. Catal., B*, 2012, **111–112**, 409–414.
- 10 Z. Shen, Z. Hu, W. Wang, S.-F. Lee, D. K. L. Chan, Y. Li, T. Gu and J. C. Yu, *Nanoscale*, 2014, **6**, 14163–14167.
- 11 H. Wang, X. Yang, W. Shao, S. Chen, J. Xie, X. Zhang, J. Wang and Y. Xie, *J. Am. Chem. Soc.*, 2015, **137**, 11376–11382.
- 12 (a) G. Fasol, *J. Phys. C: Solid State Phys.*, 1985, **18**, 1729–1741; (b) D. Li, A. E. D. R. Castillo, H. Jussila, G. Ye, Z. Ren, J. Baib, X. Chen, H. Lipsanen, Z. Suna and F. Bonaccorsoc, *Appl. Mater. Today*, 2016, **4**, 17.
- 13 C.-M. Park and H.-J. Sohn, *Adv. Mater.*, 2007, **19**, 2465–2468.
- 14 C. C. Mayorga-Martinez, N. M. Latiff, A. Y. S. Eng, Z. Sofer and M. Pumera, *Anal. Chem.*, 2016, **88**, 10074–10079.
- 15 Y. T. Yew, Z. Sofer, C. C. Mayorga-Martinez and M. Pumera, *Mater. Chem. Front.*, 2017, **1**, 1130–1136.
- 16 V. Kumar, J. R. Brent, M. Shorie, H. Kaur, G. Chadha, A. G. Thomas, E. A. Lewis, A. P. Rooney, L. Nguyen, X. L. Zhong, M. G. Burke, S. J. Haigh, A. Walton, P. D. McNaughten, A. A. Tedstone, N. Savjani, C. A. Muryn, P. O'Brien, A. K. Ganguli, D. J. Lewis and P. Sabherwal, *ACS Appl. Mater. Interfaces*, 2016, **8**, 22860–22868.
- 17 A. Ambrosi, C. K. Chua, B. Khezri, Z. Sofer, R. D. Webster and M. Pumera, *Proc. Natl. Acad. Sci. U. S. A.*, 2012, **109**, 12899–12904.
- 18 A. Ambrosi, S. Y. Chee, B. Khezri, R. D. Webster, Z. Sofer and M. Pumera, *Angew. Chem., Int. Ed.*, 2012, **51**, 500–503.
- 19 A. Ambrosi and M. Pumera, *Nanoscale*, 2014, **6**, 472–476.
- 20 G. Lupina, J. Kitzmann, I. Costina, M. Lukosius, C. Wenger, A. Wolff, S. Vaziri, M. Östling, I. Pasternak, A. Krajewska, W. Strupinski, S. Kataria, A. Gahoi, M. C. Lemme, G. Ruhl, G. Zoth, O. Luxenhofer and W. Mehr, *ACS Nano*, 2015, **9**, 4776–4785.
- 21 C. H. A. Wong, Z. Sofer, M. Kubešová, J. Kucera, S. Matejková and M. Pumera, *Proc. Natl. Acad. Sci. U. S. A.*, 2014, **111**, 13774–13779.
- 22 R. J. Toh, A. Ambrosi and M. Pumera, *Chem. – Eur. J.*, 2012, **18**, 11593–11596.
- 23 C. H. A. Wong, C. K. Chua, B. Khezri, R. D. Webster and M. Pumera, *Angew. Chem., Int. Ed.*, 2013, **52**, 8685–8688.
- 24 C. E. Banks, A. Crossley, C. Salter, S. J. Wilkins and R. G. Compton, *Angew. Chem., Int. Ed.*, 2006, **45**, 2533–2537.
- 25 W. Z. Teo and M. Pumera, *ChemPhysChem*, 2014, **15**, 3819–3023.
- 26 L. Wang and M. Pumera, *Chem. Commun.*, 2014, **50**, 12662–12664.
- 27 L. Wang, A. Ambrosi and M. Pumera, *Anal. Chem.*, 2013, **85**, 6195–6197.
- 28 L. Wang, A. Ambrosi and M. Pumera, *Electrochem. Commun.*, 2013, **26**, 71–73.
- 29 M. Pumera, A. Ambrosi and E. L. K. Chng, *Chem. Sci.*, 2012, **3**, 3347–3355.
- 30 R. Addou, S. McDonnell, D. Barrera, Z. Guo, A. Azcatl, J. Wang, H. Zhu, C. L. Hinkle, M. Quevedo-Lopez, H. N. Alshareef, L. Colombo, J. W. P. Hsu and R. M. Wallace, *ACS Nano*, 2015, **9**, 9124–9133.
- 31 R. J. Toh, Z. Sofer, J. Luxa and M. Pumera, *ChemCatChem*, 2017, **9**, 1168–1171.
- 32 A. D. F. Toy, *Comprehensive Inorganic Chemistry, The chemistry of phosphorus*, Pergamon Press, Oxford, 1975, ch. 20, pp. 398–542.
- 33 M. E. Dorfman and J. H. Hildebra, *J. Am. Chem. Soc.*, 1927, **49**, 729–737.
- 34 Y. Huang, J. Qiao, K. He, S. Bliznakov, E. Sutter, X. Chen, D. Luo, F. Meng, D. Su, J. Decker, W. Ji, R. S. Ruoff and P. Sutter, *Chem. Mater.*, 2016, **28**, 8330–8339.
- 35 V. Eswaraiah, Q. Zeng, Y. Long and Z. Liu, *Small*, 2016, **12**, 3480–3502.
- 36 S. Bagheria, N. Mansouria and E. Aghaie, *Int. J. Hydrogen Energy*, 2016, **41**, 4085–4095.
- 37 S. Lin, S. Liu, Z. Yang, Y. Li, T. W. Ng, Z. Xu, Q. Bao, J. Hao, C.-S. Lee, C. Surya, F. Yan and S. P. Lau, *Adv. Funct. Mater.*, 2016, **26**, 864–871.
- 38 D. J. Olego, J. A. Baumann, M. A. Kuck, R. Schachter, C. G. Michel and P. M. Racciah, *Solid State Commun.*, 1984, **52**, 311–314.
- 39 A. Ambrosi, A. Bonanni, Z. Sofer and M. Pumera, *Nanoscale*, 2013, **5**, 2379–2387.
- 40 W. Z. Teo and M. Pumera, *ChemElectroChem*, 2014, **1**, 249–253.

